# Phase control requirements of high intensity laser beam combining

Yan-Qi Gao,[1,*] Wei-xin Ma,[1] Bao-Qiang Zhu,[2] Dai-zhong Liu,[2] Zhao-dong Cao,[1] Jian Zhu,[1] and Ya-ping Dai[1]

[1]Shanghai Institute of Laser Plasma, Chengzhong Road, Jiading, Shanghai 201800, China

[2]Shanghai Institute of Optics and Fine Mechanics, Qinghe Road, Jiading, Shanghai 201800, China

*Corresponding author: liufenggyq@siom.ac.cn

Received 13 December 2011; revised 19 March 2012; accepted 19 March 2012; posted 19 March 2012 (Doc. ID 159896); published 16 May 2012

Aiming at getting the general requirements of the beam combine for ignition scale laser facilities, the analytical expressions including the factors affecting the combine results are derived. The physical meanings of every part are illustrated. Based on these expressions, the effects of the factors, including the beam configuration, piston error, and tip/tilt error, are studied analytically and numerically. The results show that the beam configuration cannot affect the Strehl ratio (SR) of the combined beam, but it influences the FWHM of the main peak and the ratio of the main peak and the side peak. The beam separation should be no more than 1.24 times the individual beam width for the multibeam combine, and be close to the individual beam width for the two-beam combine as much as possible. The piston error can change the characteristics of the combine beam focus, including the peak intensity, the focal spot morphology, the fractional energy contained within a certain area, and the center of mass. For the two-beam combine, a piston error less than $2\pi/5$ rad is suitable, and for the multibeam combine, the standard deviation of the piston error should be no more than $2\pi/10$ rad. The tip/tilt error has a great influence on the combined results. It affects the superposition degree of the focal spots of the combined elements directly. A requirement of $0.5 \sim 1$ $\mu$rad for the standard deviation of the tip/tilt error is adequate. 

*OCIS codes:* 140.3298, 030.1640, 140.3290, 140.3460.

## 1. Introduction

More and more experiments, such as demonstration of fast ignition, ultrahigh intensity science, plasma physics, radiography, and astrophysics, need multipetawatt, even exawatt, laser facility urgently [1–6]. Many efforts have been made to improve the laser intensity, especially on the aspects of the meter scale grating (multilayer dielectric grating and gold grating) [7,8] and the grating tiling [9–13]. However, the limited beam size is still a huge obstacle to improve the laser intensity. Laser beam combing, especially the coherent beam combing, offers an excellent method to expand the usable beam size [14]. The coherent beam combing is to combine many small sizes of laser beams that are phasing with one another. Its essence is to make many small-size laser beams act as a huge-size beam without degrading the beam quality markedly. It has been studied widely these years [15–19], though these studies focused mostly on the fiber laser and solid state laser, which aim at higher average power. Fortunately, the advantages of coherent beam combing have been noticed by researchers dreaming of improving beam intensity, and many ignition scale. facilities have been planned or considered to use this technique [20]. Researchers at the Lawrence Livermore National Laboratory (LLNL) plan to transform one quad of the National Ignition Facility (NIF) beams (four beam pairs) to advanced radiography capability (ARC) beams used for diagnostics and fast ignition experiments [21].

1559-128X/12/152941-10$15.00/0

The four beam pairs (2 × 2) are coherently combined to obtain 4 kJ within a 40 $\mu$m diameter circle. Excellent work on such topics as phase measurements [22], phase controls [23,24], and dispersion effects [25] have been done. The PETAL laser facility, which is being built near Bordeaux, in France, is a multipetawatt high-energy laser [26]. The beam-combing techniques in this facility have a different version. In the second stage of its compressor, the whole large beam is divided into four segments (1 × 4) in order to overcome the limitation of grating size. They are compressed separately and then combined coherently [27]. In order to achieve better combine results for a shorter pulse duration (500 fs), much innovative work has been done in areas such as synchronization measurement using a 2D spectral interferometer [28], piston and tilt measurement using a quadrilateral wavefront interferometer [29], longitudinal chromatism measurement basing on 2D spectral interferometer [30], and longitudinal chromatism compensation using refractive lenses [31]. FIREX-I, built at Osaka University (Japan) is also planned to combine four laser beams (2 × 2) to achieve 10 kJ/10 ps output for fast ignition experiments [32]. The forthcoming HiPER facility and ELI-NP facility also take coherent beam combing as an important developing option [33,34]. However, coherent beam combing is still a great challenge for ignition scale facilities, and a great deal more work needs to be done on the combing theories, error measurements, and error controls.

This work aims at putting forward the phase control requirements of the coherent beam combing for ignition scale facilities systematically, which is insufficient or neglected in previous works. This paper is organized as follows. In Section 2, the effects of beam configuration on the combined focus are analyzed based on the analytical expressions. Then, the influences of the piston errors on the combined results are presented in Section 3. Next, the degeneration of the combine focus due to the tip/tilt errors is illustrated. Finally, the conclusions are outlined.

## 2. Beam Configuration and Coherent Beam Combing

In this section, we present the essence of the coherent beam combine based on the analytical expression derivation, and the factors affecting the combine results are analyzed.

For $M \times N$ beam combines, we can write the input beam function as

$$E(x,y) = \sum_{m=1}^{M}\sum_{n=1}^{N} E_{mn}(x,y)\exp[i\phi_{mn}(x,y)], \quad (1)$$

where $E_{mn}(x,y)$ and $\exp[i\phi_{mn}(x,y)]$ represent the amplitude and phase of the individual beam, respectively. In the following analysis, we assume that each beam has the same rectangular aperture, as shown in Fig. 1, and the amplitude can be expressed as

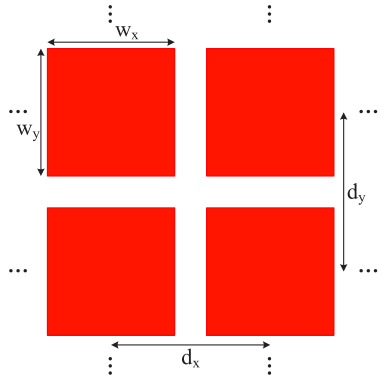


Fig. 1. (Color online) Schematic diagram of the beam configuration for coherent beam combine.

$$E_{mn}(x,y) = \mathrm{rect}\left(\frac{x-md_x}{w_x}\right) \times \mathrm{rect}\left(\frac{y-nd_y}{w_y}\right), \quad (2)$$

where $w$ and $d$ denote the beam width and beam separation, respectively, and $m$ and $n$ mean the beam sequence numbers. If the individual beams have the same phase, in other words, they are phased with each other, the phase term can be ignored, and the input beam function can be expressed as

$$E(x,y) = E_{00}(x,y) \otimes \sum_{m=1}^{M}\sum_{n=1}^{N} \delta(x-md_x)\delta(y-nd_y), \quad (3)$$

where $\otimes$ is the convolution operator. Ignoring the scale factor $1/\lambda f$ of focal plan coordinate, the electric field distribution in the focal plane can be expressed as [35]

$$\begin{aligned} U(f_x,f_y) &= \frac{1}{\lambda f}\int E(x,y)\exp[-2\pi i(f_x x + f_y y)]\mathrm{d}x\mathrm{d}y \\ &= \frac{w_x w_y MN}{\lambda f} \times F\left[\frac{1}{w_x w_y}E_{00}(x,y)\right] \\ &\quad \times \frac{1}{MN}\sum_{m=1}^{M}\sum_{n=1}^{N}\exp(2\pi i m d_x f_x + 2\pi i n d_y f_y) \\ &= \frac{w_x w_y MN}{\lambda f} \times P(f_x,f_y) \times G(f_x,f_y), \end{aligned} \quad (4)$$

in which $\lambda$ is the wavelength, $f$ denotes the focal length of the lens, $(f_x,f_y)$ is the normalized coordinate of the focal plane, and $F$ means Fourier transform. The intensity distribution in the focal plane is

$$\begin{aligned} I(f_x,f_y) &= |U(f_x,f_y)|^2 \\ &= \left(\frac{w_x w_y MN}{\lambda f}\right)^2 \times \mathrm{PSF}(f_x,f_y) \times \mathrm{GF}(f_x,f_y). \end{aligned} \quad (5)$$

As shown in Eq. (5), the far-field intensity distribution of the coherent beam combine for the phased beams can be written as three parts: a scale factor $(w_x w_y MN/\lambda f)^2$, a point spread function of individual beam $\mathrm{PSF}(f_x,f_y)$, and a grid function $\mathrm{GF}(f_x,f_y)$.

Substituting Eq. (2) into Eq. (5), we can get the far-field intensity distribution of rectangular beam combine. Its PSF can be written as

$$\mathrm{PSF}(f_x, f_y) = \mathrm{sinc}^2(w_x f_x)\mathrm{sinc}^2(w_y f_y). \quad (6)$$

Here, the sinc function stands for normalized sinc function $\mathrm{sinc}(x) = \sin(\pi x)/(\pi x)$. The grid function can be simplified as

$$\mathrm{GF}(f_x, f_y) = \frac{1}{(MN)^2} \frac{\sin^2(\pi M d_x f_x)}{\sin^2(\pi d f_x)} \frac{\sin^2(\pi N d_y f_y)}{\sin^2(\pi d f_y)}. \quad (7)$$

Figure 2 illustrates the characteristics of the PSF, GF, and normalized intensity distribution. In Fig. 2(a), the PSF denotes the point spread function, and the other two lines indicate the evolution of the grid function with the beam separation. Figure 2(c) shows the evolution of the grid function with the beam combine number. In these figures, the individual beam width is set as $1 \times 1$; the beam combing number is $2 \times 2$. From Fig. 2 and Eqs. (5–7), we can obtain several important characteristics about coherent beam combine without errors. First, the peak intensity, which could be gotten by setting $f_x = f_y = 0$, is affected only by the scale factor $(w_x w_y MN/\lambda f)^2$, having nothing to do with the PSF and GF, because the maximum values of the PSF and GF are both 1. That is to say, the Strehl ratio, defined as the ratio of the peak far-field intensity of a combined beam and the peak far-field intensity of an equative whole large beam with uniform intensity and wave front distribution, is always 1 for the phasing beam, and has nothing to do with the beam configuration. The scale factor decides the maximum

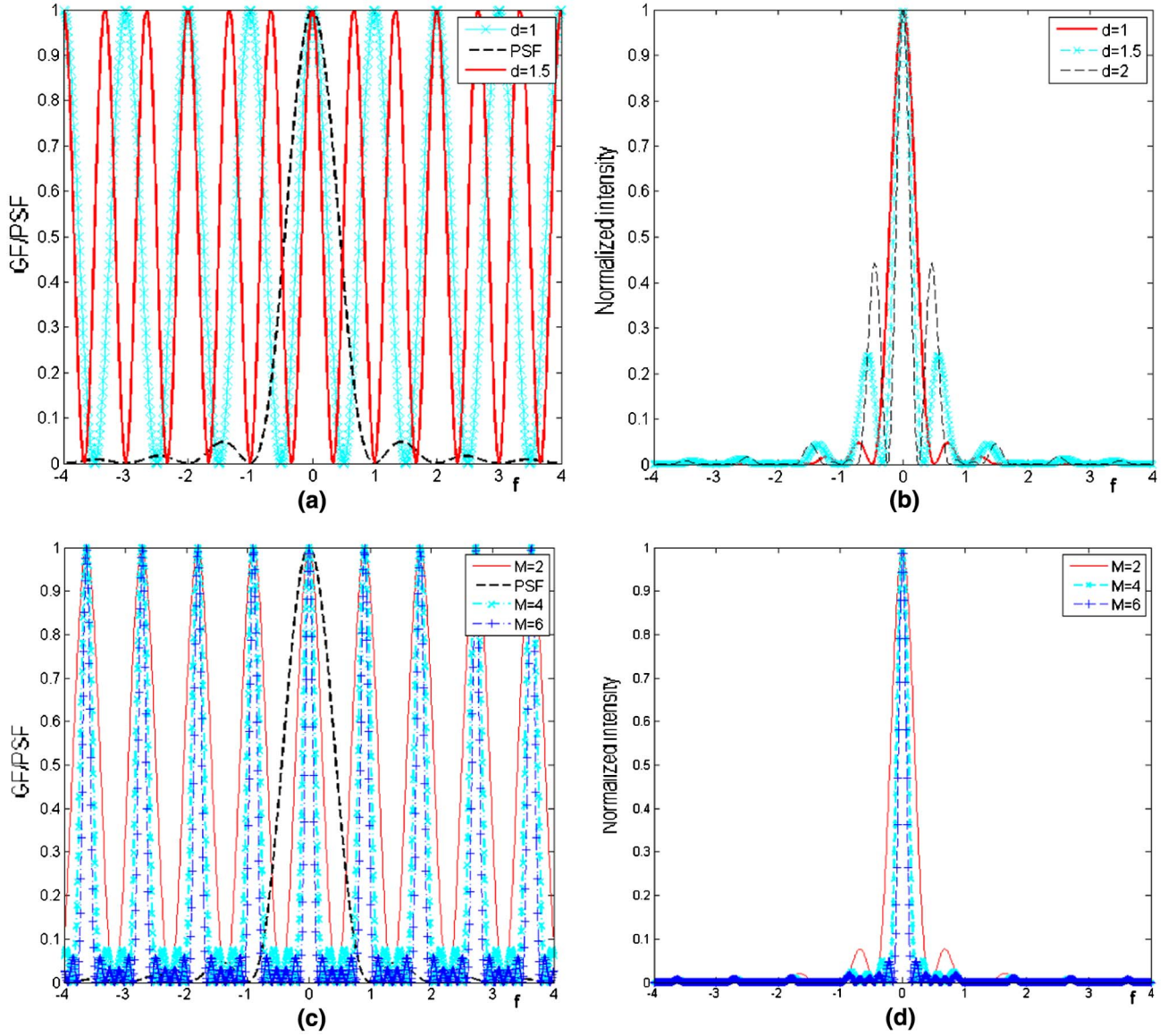


Fig. 2. (Color online) (a) and (c) illustrate the PSF, GF, and (b) and (d) indicate normalized far-field intensity distribution, (a) and (b) with different beam separation when $M = N = 2$, (c) and (d) with different beam number when $d = 1.1$.

intensity, which can be achieved by beam combine. Second, the grid function GF is a periodic function with a maximum value of 1 and a period of $T_x = 1/d_x$, both of which are independent of the combine beam number $m,n$. It decides the spike number, intensity, and location within the area corresponding to the one-time diffraction limit of the individual beam. Third, the point spread function PSF decides the envelope of the combined focal spot. Fourth, the beam combine number affects the shape of the spike, mostly the full width at half maximum (FWHM) of the spike.

According to the above four points, we can decide the beam configuration based on the system requirements. Take the square beam combine as an example. The beam combine number $M \times N$ and individual beam area $w_x w_y$ can been chosen based on the scale factor $(w_x w_y MN/\lambda f)^2$. For ignition scale facilities, we always pursue the focusability. If it is required that the second maximum peak value of the combined focal spot be no more than 0.05 times the maximum peak value (this requirement corresponds to the situation of a whole ideal beam's focal spot), then the beam separation distance should satisfied $\mathrm{sinc}^2(w_x/d_x) < 0.05$, and we can get the conclusion that $d_x < 1.24 w_x$. For a small number beam combines, such as $2 \times 2$, the locations of the peaks move toward the center, and the second maximum peak increases with the increase of the $d_x$, so, the beam separation distance $d_x$ should be close to the beam width $w_x$ as much as possible.

### 3. Piston Error and Coherent Beam Combing

If we suppose that the individual beams have a uniform phase $\Phi_{mn}$ but are different from each other, the input beam function can be rewritten as

$$E(x,y) = E_{00}(x,y) \otimes \sum_{m=1}^{M}\sum_{n=1}^{N} \delta(x - md_x)\delta(y - nd_y)\exp(i\Phi_{mn}). \tag{8}$$

The phase difference $\Delta\Phi_{mn}$ between the individual beam and the mean value is called piston error. With the piston error, the electric field distribution in the focal plane becomes

$$\begin{aligned} U(f_x,f_y) &= \frac{w_x w_y MN}{\lambda f} \times F\left[\frac{1}{w_x w_y} E_{00}(x,y)\right] \\ &\quad \times \frac{1}{MN}\sum_{m=1}^{M}\sum_{n=1}^{N} \exp(2\pi i m d_x f_x \\ &\quad + 2\pi i n d_y f_y)\exp(i\Phi_{mn}) \\ &= \frac{w_x w_y MN}{\lambda f} \times P(f_x,f_y) \times G_p(f_x,f_y). \end{aligned} \tag{9}$$

The intensity distribution in the focal plane has the same form with Eq. (5) except the factor GF:

$$\begin{aligned} I(f_x,f_y) &= |U(f_x,f_y)|^2 \\ &= \left(\frac{w_x w_y MN}{\lambda f}\right)^2 \times \mathrm{PSF}(f_x,f_y) \times \mathrm{GF}_p(f_x,f_y). \end{aligned} \tag{10}$$

In Section 2, we have demonstrated that the three parts, scale factor $(w_x w_y MN/\lambda f)^2$, the grid function GF, and the point spread function PSF, denote different physical meanings. From Eqs. (9) and (10), we can find that the piston error affects just the grid function $\mathrm{GF}_p(f_x,f_y)$. Hence, we need only to analyze the influence of the piston error on the grid function.

In order to simplify the analysis, the grid function of a $1 \times 2$ beam combine with piston error is presented first. These two beams are all square. In this case, the grid function can be written as

$$\begin{aligned} \mathrm{GF}_p(f_x,f_y) = \Big| &\frac{1}{2} \times \exp(2\pi i d f_x) \times [\exp(2\pi i d f_y) \\ &+ \exp(2 \times 2\pi i d f_y)\exp(i\phi)]\Big|^2, \end{aligned} \tag{11}$$

where, $\phi$ indicates the phase different between the two beams. After simplification, Eq. (11) becomes

$$\mathrm{GF}_p(f_x,f_y) = \frac{1}{4} \times \frac{\sin^2(2\pi d f_y + \phi)}{\sin^2(\pi d f_y + \phi/2)}. \tag{12}$$

It is found that the period of the grid function $\mathrm{GF}_p$ is still $T = 1/d$, and its maximum value is still 1, just adding a transverse translation $-\phi/(2\pi d)$. Because of the translation, the position of its maximum value is changed. As a result, the maximum value and the morphology of the combined focal spot are changed.

Figure 3 shows the results of two square beam combines with different piston errors using the above analytical results Eqs. (10–12). In Fig. 3(a), the PSF denotes the point spread function, and the other four lines indicate the evolution of the grid functions with different piston errors $\phi$. Because of the transverse translation of the grid function, the combined focus is changed significantly, as shown in Figs. 3(b) and 3(c). Four important characteristic quantities of the focal spot—which are the peak intensity, the focal spot morphology, the fractional energy contained within the 1 times diffraction limit area, and the center of mass—are changed because of the piston error. All four of these characteristic quantities can be gotten based on the above analytical results, Eqs. (10–12). More importantly, the above four quantities offer several ways to eliminate the piston error in phasing the combined beam. A different version is presented in [23].

Figure 4 gives the Strehl ratio (SR), the fractional energy contained (FEC) within the square area corresponding to 1 times diffraction limit, the ratio of the second peak and main peak (RSM), and the center of mass (CM) as a function of piston error. If we choose the following requirements—SR > 0.9,

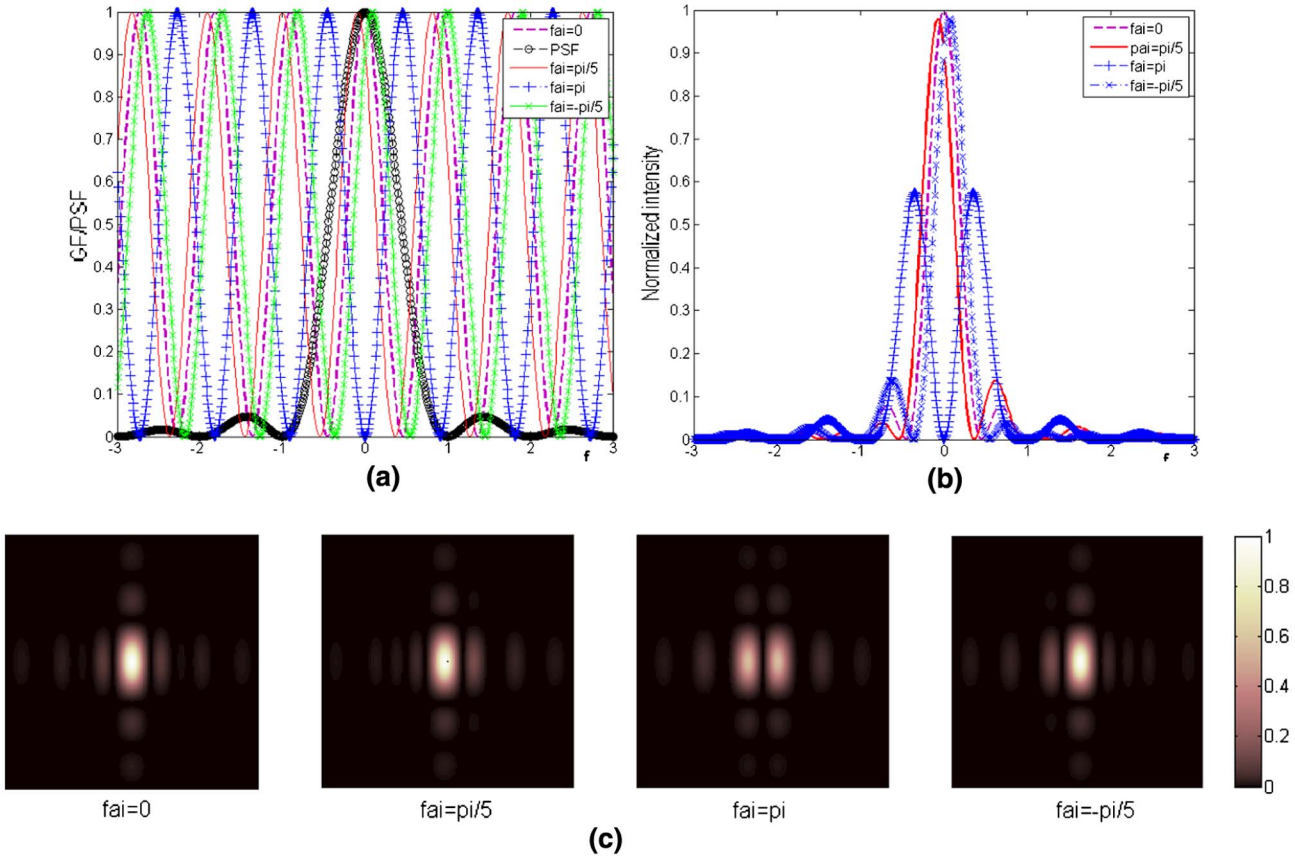


Fig. 3. (Color online) (a) PSF, GF and (b) normalized far-field intensity distribution with different piston error $\phi$ when $d = 1.1$, (c) the 2D image of focal spots corresponding to the four cases shown in (a) and (b).

FEC > 0.7, RSM < 0.2, CM < 0.15—as an example, then the piston must be phased to less than $2\pi/5$.

For a multibeam combine, the grid function $GF_p(f_x, f_y)$ becomes complicated because of the random piston error of the individual beams. Figure 5 illustrates the grid function of 10 × 10 beam combine when piston errors obey normal distribution with a mean of zero and a standard deviation of 0, $0.2\pi$, $0.4\pi$, and $0.6\pi$, respectively. Figure 6 gives the normalized intensity distribution based on the cases shown in Figs. 5(b), 5(c), and 5(d). It is found that the peak intensity decreases rapidly as the piston error

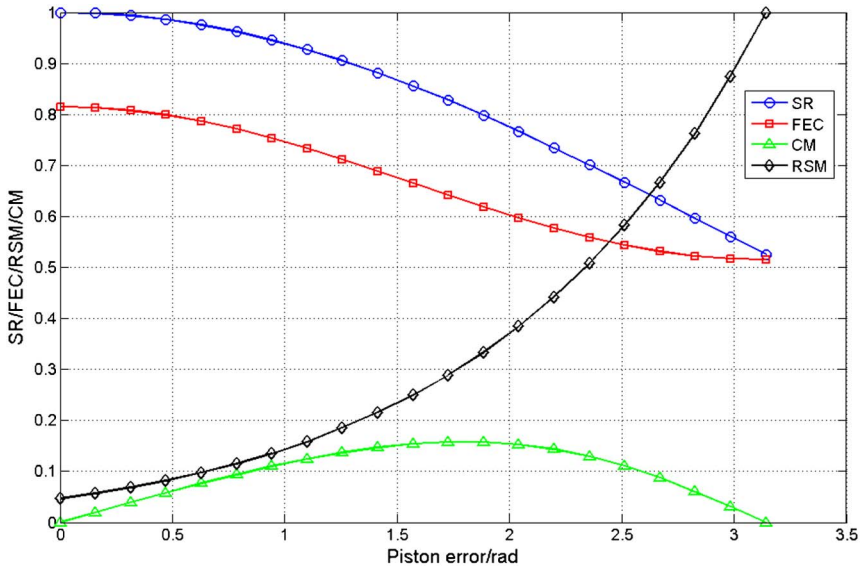


Fig. 4. (Color online) SR, FEC, RSM, and CM as a function of piston error.

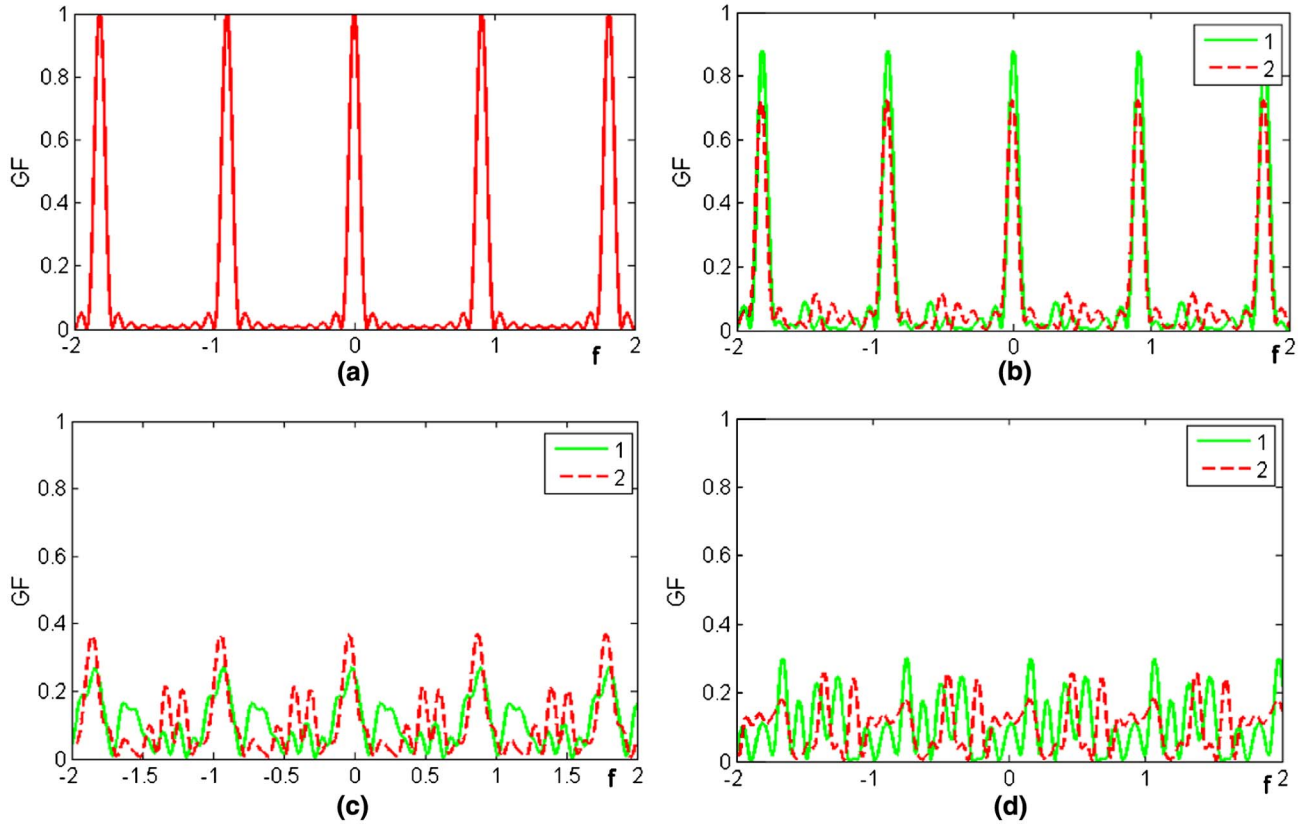


Fig. 5. (Color online) Grid function of 10 × 10 beam combine; piston errors obey normal distribution with a mean of zero and a standard deviation of (a) 0, (b) $0.2\pi$, (c) $0.4\pi$, and (d) $0.6\pi$. The numbers "1" and "2" indicate the two random dates.

increase, and the peak intensities might be greatly different even for the pistons with the same standard deviation. In order to study the characteristics of this situation, the ensemble averaged focal spot intensity is used:

$$\langle I(f_x,f_y)\rangle = \frac{(w_x w_y MN)^2}{\lambda^2 f^2} \times |P(f_x,f_y)|^2 \times \langle |G_p(f_x,f_y)|^2 \rangle = \frac{(w_x w_y MN)^2}{\lambda^2 f^2} \times \mathrm{PSF}(f_x,f_y) \times \mathrm{GF}_{\mathrm{ea}}(f_x,f_y). \quad (13)$$

As shown in Eq. (13), we just need take care of the grid function $\mathrm{GF}_{\mathrm{ea}}(f_x,f_y)$. Borrowing the calculation method used for the large segmented telescopes analysis, the grid function can be written as [36–39]

$$\mathrm{GF}_{\mathrm{ea}}(f_x,f_y) = \exp(-\sigma^2)\mathrm{GF}(f_x,f_y) + MN[1-\exp(-\sigma^2)], \quad (14)$$

where $\sigma$ is the standard deviation of the piston error, and the piston error is supposed to obey normal

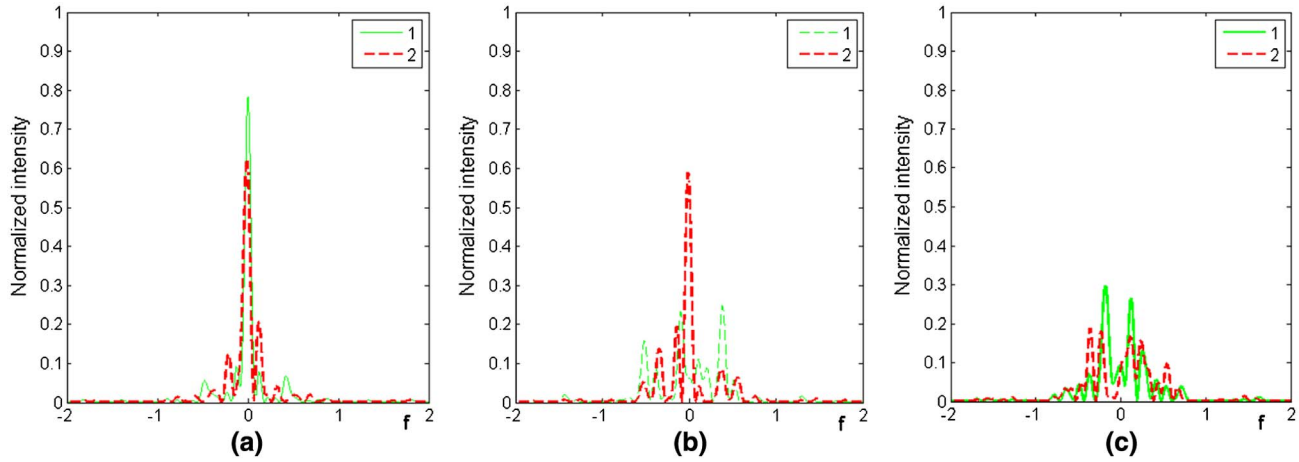


Fig. 6. (Color online) Normalized intensity distribution of 10 × 10 beam combine, (a), (b), and (c) corresponding to the situations of (b), (c), and (d) in Fig. 5 respectively.

distribution with a mean of zero. The Strehl ratio becomes

$$S = \frac{\mathrm{GF}_{\mathrm{ea}}(0,0)}{\mathrm{GF}(0,0)} = \frac{1}{MN}[1 + (MN-1)\exp(-\sigma^2)]. \quad (15)$$

Obviously, when $\sigma \to 0$, $S \to 1$, which corresponds to coherent combine ideally, and when $\sigma \to \infty$, $S \to 1/MN$, which means incoherent combine.

Figure 7 illustrates the Strehl ratio and the fractional energy contained within a square area (FEC) as functions of the standard deviation of piston errors for the $10 \times 10$ beam combine. For every sampling point, we choose 50 values randomly. The bars indicate the range of the 50 values for every sampling point. The lines plot the means of every point. 1DL and 5DL mean that the square areas used for the FEC calculation are 1 or 5 times the diffraction limits of the combined beam. The "stat." and "Eq." indicate that the lines of the SR are gotten based on the statistic calculations or Eq. (15). The results show that both the SR and FEC decrease rapidly with the increase of the standard deviation, and the uncertainty of both increase. For instance, if we want to control the SR $> 0.7$, and the FEC within the 5DL area is no less than 70% for the multibeam combine, then the standard deviation of the piston error should be no more than $2\pi/10$ rad.

#### 4. Tip/Tilt and Coherent Beam Combing

For the coherent beam combine, another important factor greatly affecting the combining results is the uniformity of the individual beam pointing. It is decided by the tip/tilt error of the individual beam. The uniformity of the individual beam pointing or tip/tilt error can be understood as the overlap degree of the individual beam focus simply. This section will reveal the effects of the tip/tilt errors on the beam combine.

The tip/tilt errors can be represented by the rotation of the wave front around the $x$ axis or $y$ axis by an angle $\alpha_x$ or $\alpha_y$ (the $x$-$y$ plane is the ideal wavefront plane). Hence, the wavefront of the tip/tilt beam can be written as

$$\Phi_{mn}(x,y) = \frac{2\pi}{\lambda} \times (\alpha_x, \alpha_y) \bullet (x - md_x, y - nd_y). \quad (16)$$

Comparing with Eq. (8), it is found that the phase factor $\Phi_{mn}$ becomes a function of the coordinate $(x,y)$. So the input electric field cannot be written as the convolution form like Eq. (8), and we can only start from

$$U(f_x,f_y) = \frac{1}{\lambda f}\int E(x,y)\exp[-2\pi i(f_x x + f_y y)]\mathrm{d}x\mathrm{d}y. \quad (17)$$

Substituting Eqs. (1) and (16) into Eq. (17), after calculation and simplification, we can get

$$\begin{aligned} U(f_x,f_y) = \frac{1}{\lambda f}\sum_{m=1}^{M}\sum_{n=1}^{N} &\exp[-2\pi i(f'_x,f'_y) \\ &\bullet (md,nd)]\exp\left[-\frac{2\pi i}{\lambda}(\alpha_{mnx}md, \alpha_{mny}nd)\right] \\ &\times \int E_0(x',y')\exp[-2\pi i(f'_x,f'_y) \\ &\bullet (x',y')]\mathrm{d}x'\mathrm{d}y', \end{aligned} \quad (18)$$

where $(x',y') = (x - md_x, y - nd_y)$, and $(f'_x,f'_y) = \left(f_x - \frac{\alpha_{mnx}}{\lambda}, f_y - \frac{\alpha_{mny}}{\lambda}\right)$. Then, the intensity of the combined focal spot becomes

$$\begin{aligned} I(f'_x,f'_y) = \left(\frac{1}{\lambda f}\right)^2 \Bigg| &\sum_{m=1}^{M}\sum_{n=1}^{N}\exp[-2\pi i(f'_x,f'_y) \\ &\bullet (md,nd)]\exp\left[-\frac{2\pi i}{\lambda}(\alpha_{mnx}md, \alpha_{mny}nd)\right] \\ &\times \int E_0(x',y')\exp[-2\pi i(f'_x,f'_y) \bullet (x',y')]\mathrm{d}x'\mathrm{d}y'\Bigg|^2. \end{aligned} \quad (19)$$

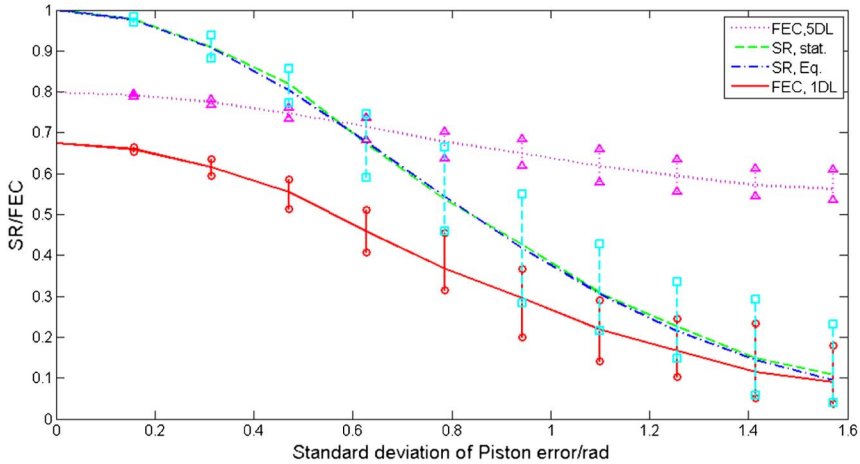


Fig. 7. (Color online) Strehl ratio (SR) and the fractional energy contained within a square area (FEC) of the $10 \times 10$ beam combine as functions of the standard deviation of piston errors.

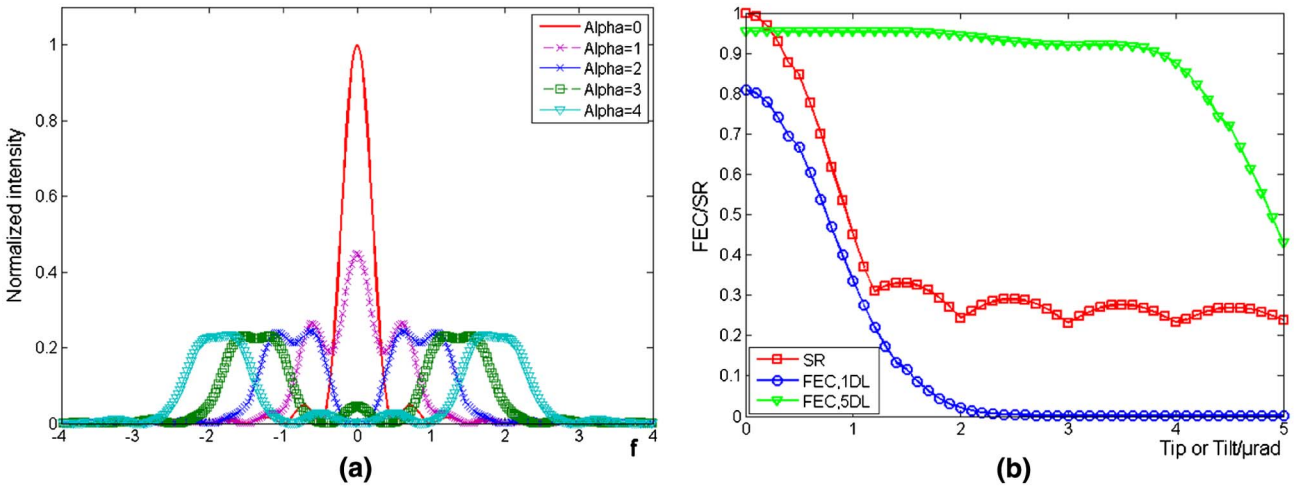


Fig. 8. (Color online) Combine results of the $1 \times 2$ beams with different tip/tilt errors. (a) Focal spot intensity distributions with different tip/tilt errors; (b) the SR and FEC as a function of tip/tilt error.

Because the $(x', y')$ and $(f'_x, f'_y)$ are related with $(m, n)$, Eq. (19) cannot be written as three independent parts, as Eq. (10). However, every factor of Eq. (19) still has obvious physical meaning. For the $(m, n)$ order beam, the effects of the tip/tilt error on its focal spot have two main points: first, the change of the phase $\frac{2\pi i}{\lambda}(\alpha_{mnx} md + \alpha_{mny} nd)$; second, the change of the location $(f_x - \frac{\alpha_{mnx}}{\lambda}, f_y - \frac{\alpha_{mny}}{\lambda})$. From the above two points, we can find that the effects of the tip/tilt error on the combined results are just related to the combine parameter $d$ and tip/tilt error $\alpha$.

Figure 8 shows the $1 \times 2$ beam combine results with different tip/tilt errors based on Eq. (19). The alpha with unit "$\mu$rad" means the angle between the two beams. Figure 8(a) shows the focal spot intensity distributions with different tip/tilt errors, and Fig. 8(b) shows the SR, FEC within the area of one time diffraction limit, and the FEC within the area of five times diffraction limit. The SR is very sensitive to the tip/tilt errors, because this kind of error separates the individual focus directly. For the calculations shown in Fig. 8, the angle $\alpha$ between the two beams is divided equally, and the "0" position corresponds to angular bisector. If we want to get the SR $> 0.8$, the tip/tilt error should be no more than 0.5 $\mu$rad. This requirement is very harsh for the ignition scale facilities. Because of numerous optical elements, especially lots of mirrors, the pointing stability of the final output bean is often not better than 5 $\mu$rad [40–42]. Hence, the requirement of beam combine on the beam pointing stability is a big challenge.

Figure 9 gives the SR as a function of the standard deviation of the tip/tilt error for different numbers of beam combine. The numbers "5" or "10" indicate the combined beam number. For every point, 50 results are calculated randomly. The lines are plotted using the mean value of every point. The ranges indicating by the bar stand for the jitter of the 50 results for the corresponding point. We can find that the mean value of SR is close to $1/N$, where $N$ is the beam combine number, when the standard deviation is about 1 $\mu$rad. The SR value $1/N$ corresponds to the incoherent beam combine result without tip/tilt error. It should be noticed that the SR for different beam combine

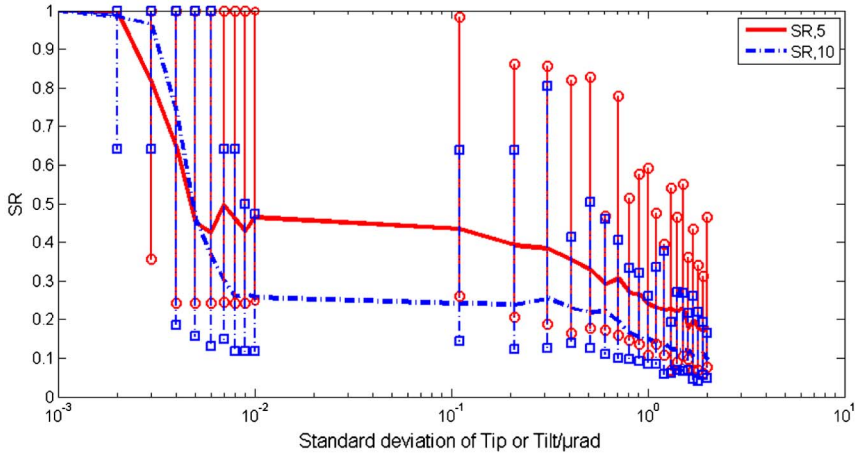


Fig. 9. (Color online) SR as a function of tip/tilt error; the number means the number of combined beams.

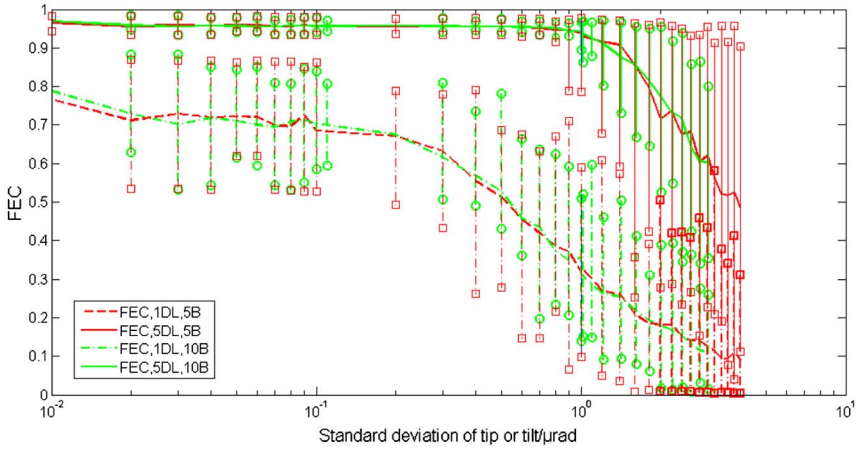


Fig. 10. (Color online) FEC as a function of tip/tilt error. The first number indicate times of diffraction limit used for the FEC calculation; the second number means the number of combined beams.

number has different mean values even the standard deviation is same. Generally, for the same standard deviation, the bigger the beam combine number is, the smaller the SR is. But it does not mean that the combine result is worse. For example, when the standard deviation of tip/tilt error is 1 $\mu$rad, the SRs are about 0.25 and 0.14 for 5 beams combined and 10 beams combined, respectively. The peak intensity of combined focal spot is 6.25 (or 14.00) times of that of the individual beam focal spot for 5 (or 10) beams combined. The two results are all bigger than the maximum focal spot intensity, which could be achieved by the incoherent beam combine using the corresponding beam number even without tip/tilt error. Figure 10 illustrates the FEC within the areas of 1 time diffraction limit and that of the 5 times diffraction limit for the different standard deviation of tip/tilt errors. Using the results shown in Fig. 9 and Fig. 10, the beam combine tip/tilt demands of the ignition scale facility can be gotten for a specific system requirement. Generally, it is demanded that the maximum intensity and the focusability of the combined focus are much better than those that could be achieved by the incoherent beam combine, and the above two factors are stability enough for every fire. A requirement of $0.5 \sim 1$ $\mu$rad for the standard deviation of the tip/tilt error is adequate.

## 5. Conclusions

In order to get the general requirements of the beam combine for the ignition scale facility, the analytical expressions including the factors affecting the combine results are derived. Based on these expressions, the influences of the factors, including the beam configuration, piston error, and tip/tilt error, are studied analytically and numerically. The results show that the beam configuration cannot affect the SR of the combined beam, but it influences the FWHM of the main peak, as well as the ratio of the side peak and the main peak. It should be controlled. The piston error affects the grid function greatly, including its maximum value, transverse translation, and formation. Hence, the piston error can change the characteristics of the combine beam focus, including the peak intensity, the focal spot morphology, the fractional energy contained within a certain area, and the center of mass. For the two-beam combine, a piston error less than $2\pi/5$ rad is suitable, and for a multibeam combine, the standard deviation of the piston error should be no more than $2\pi/10$ rad (this can be adjusted based on focal spot requirement). The tip/tilt error has great influences on the combined results. It affects the degree of the superposition of the individual focal spot directly. If we want to get the SR $> 0.8$, the tip/tilt error should be no more than 0.5 $\mu$rad for the two-beam combine. For the multibeam combine, a standard deviation no more than $0.5 \sim 1$ $\mu$rad is appropriate.

Above these requirements, the piston error and tip/tilt error control are most difficult, considering the numerous optic elements using in the ignition scale facility. Fortunately, the adapted optics (kinds of deformable mirrors) and active point control techniques might offer good potential solutions.

## References

1. M. Tabak, D. S. Clark, S. P. Hatchett, M. H. Key, B. F. Lasinski, R. A. Snavely, S. C. Wilks, R. P. J. Town, R. Stephens, E. M. Campbell, R. Kodama, K. Mima, K. A. Tanaka, S. Atzeni, and R. Freeman, "Review of progress in fast ignition," Phys. Plasmas **12**, 057305 (2005).
2. J. D. Zuegel, S. Borneis, C. Barty, B. Legarrec, C. Danson, N. Miyanaga, P. K. Rambo, C. Leblanc, T. J. Kessler, A. W. Schmid, L. J. Waxer, J. H. Kelly, B. Kruschwitz, R. Jungquist, E. Moses, J. Britten, I. Jovanovic, J. Dawson, and N. Blanchot, "Laser challenges for fast ignition," Fusion Sci. Technol. **49**, 453–482 (2006).
3. M. Roth, T. E. Cowan, M. H. Key, S. P. Hatchett, C. Brown, W. Fountain, J. Johnson, D. M. Pennington, R. A. Snavely, S. C. Wilks, K. Yasuike, H. Ruhl, F. Pegoraro, S. V. Bulanov, E. M. Campbell, M. D. Perry, and H. Powell, "Fast ignition by intense laser-accelerated proton beams," Phys. Rev. Lett. **86**, 436–439 (2001).
4. Michael Schirber, "For nuclear fusion, could two lasers be better than one?" Science **310**, 1610–1611 (2005).
5. M. H. Key, "Status of and prospects for the fast ignition inertial fusion concept," Phys. Plasmas **14**, 055502 (2007).
6. M. Dunne, "A high-power laser fusion facility for Europe," Nat. Phys. **2**, 2–5 (2006).

7. H. T. Nguyen, J. A. Britten, T. C. Carlson, J. D. Nissen, L. J. Summers, C. R. Hoaglan, M. D. Aasen, J. E. Peterson, and I. Jovanovic, "Gratings for high-energy petawatt lasers," Proc. SPIE **5991**, 59911M (2005).
8. J. A. Britten, H. T. Nguyen, L. M. Jones II, T. C. Carlson, C. R. Hoaglan, L. J. Summers, M. D. Aasen, A. Rigatti, and J. Oliver, "First demonstration of a meter-scale multilayer dielectric reflection grating for high-energy petawatt-class lasers," Lawrence Livermore National Laboratory, UCRL-JRNL-205887 (2004).
9. T. J. Kessler, J. Bunkenburg, H. Huang, A. Kozlov, and D. D. Meyerhofer, "Demonstration of coherent addition of multiple gratings for high-energy chirped-pulse-amplified lasers," Opt. Lett. **29**, 635–637 (2004).
10. J. Qiao, A. Kalb, T. Nguyen, J. Bunkenburg, D. Canning, and J. H. Kelly, "Demonstration of large-aperture tiled-grating compressors for high-energy, petawatt-class, chirped-pulse amplification systems," Opt. Lett. **33**, 1684–1686 (2008).
11. H. Habara, G. Xu, T. Jitsuno, R. Kodama, K. Suzuki, K. Sawai, K. Kondo, N. Miyanaga, K. A. Tanaka, K. Mima, M. C. Rushford, J. A. Britten, and C. P. J. Barty, "Pulse compression and beam focusing with segmented diffraction gratings in a high-power chirped-pulse amplification glass laser system," Opt. Lett. **35**, 1783–1785 (2010).
12. J. Qiao, A. Kalb, M. J. Guardalben, G. King, D. Canning, and J. H. Kelly, "Large-aperture grating tiling by interferometry for petawatt chirped-pulse—amplification systems," Opt. Express **15**, 9562–9574 (2007).
13. M. Hornung, R. Bödefeld, A. Kessler, J. Hein, and M. C. Kaluza, "Spectrally resolved and phase-sensitive far-field measurement for the coherent addition of laser pulses in a tiled grating compressor," Opt. Lett. **35**, 2073–2075 (2010).
14. T. Y. Fan, "Laser beam combining for high-power, high-radiance sources," IEEE J. Sel. Top. Quantum Electron. **11**, 567–577 (2005).
15. L. Daniault, M. Hanna, D. N. Papadopoulos, Y. Zaouter, E. Mottay, F. Druon, and P. Georges, "Passive coherent beam combining of two femtosecond fiber chirped-pulse amplifiers," Opt. Lett. **36**, 4023–4025 (2011).
16. S. M. Redmond, K. J. Creedon, J. E. Kansky, S. J. Augst, L. J. Missaggia, M. K. Connors, R. K. Huang, B. Chann, T. Y. Fan, G. W. Turner, and A. Sanchez-Rubio, "Active coherent beam combining of diode lasers," Opt. Lett. **36**, 999–1001 (2011).
17. T. Weyrauch, M. A. Vorontsov, G. W. Carhart, L. A. Beresnev, A. P. Rostov, E. E. Polnau, and J. J. Liu, "Experimental demonstration of coherent beam combining over a 7 km propagation path," Opt. Lett. **36**, 4455–4457 (2011).
18. G. D. Goodno, H. Komine, S. J. McNaught, S. B. Weiss, S. Redmond, W. Long, R. Simpson, E. C. Cheung, D. Howland, P. Epp, M. Weber, M. McClellan, J. Sollee, and H. Injeyan, "Coherent combination of high-power, zigzag slab lasers," Opt. Lett. **31**, 1247–1249 (2006).
19. Y. Zheng, X. Wang, L. Deng, F. Shen, and X. Li, "Arbitrary phasing technique for two-dimensional coherent laser array based on an active segmented mirror," Appl. Opt. **50**, 2239–2245 (2011).
20. M. H. Key, "Status of and prospects for the fast ignition inertial fusion concept," Phys. Plasmas **14**, 055502 (2007).
21. C. P. J. Barty, M. H. Key, J. Britten, R. Beach, G. Beer, C. Brown, S. Bryan, J. Caird, T. Carlson, J. Crane, J. Dawson, A. C. Erlandson, D. Fittinghoff, M. Hermann, C. Hoaglan, A. Iyer, L. Jones II, I. Jovanovic, A. Komashko, O. Landen, Z. Liao, W. Molander, S. Mitchell, E. Moses, N. Nielsen, H-H. Nguyen, J. Nissen, S. Payne, D. Pennington, L. Risinger, M. Rushford, K. Skulina, M. Spaeth, B. Stuart, G. Tietbohl, and B. Wattellier, "An overview of LLNL high-energy short-pulse technology for advanced radiography of laser fusion experiments," Nucl. Fusion **44**, S266 (2004).
22. K. L. Baker, "Interferometric adaptive optics for high-power laser pointing and wavefront control and phasing," J. Micro-Nanolith. Mem. **8**, 033040 (2009).
23. K. L. Baker, D. Homoelle, E. Utterback, and S. M. Jones, "Phasing rectangular apertures," Opt. Express **17**, 19551–19565 (2009).
24. K. L. Baker, D. Homoelle, E. Utternback, E. A. Stappaerts, C. W. Siders, and C. P. J. Barty, "Interferometric adaptive optics testbed for laser pointing, wave-front control and phasing," Opt. Express **17**, 16696–16709 (2009).
25. D. Homoelle, J. K. Crane, M. Shverdin, C. L. Haefner, and C. W. Siders, "Phasing beams with different dispersions and application to the petawatt-class beamline at the National Ignition Facility," Appl. Opt. **50**, 554–561 (2011).
26. N. Blanchot, G. Behar, T. Berthier, E. Bignon, F. Boubault, C. Chappuis, H. Coïc, C. Damiens-Dupont, J. Ebrardt, O. Flour, Y. Gautheron, P. Gibert, O. Hartmann, E. Hugonnot, F. Laborde, D. Lebeaux, J. Luce, S. Montant, S. Noailles, J. Néauport, D. Raffestin, A. Roques, F. Sautarel, M. Sautet, C. Sauteret, and C. Rouyer, "Overview of PETAL, the multi-Petawatt project on the LIL facility," Plasma Phys. Contr. F. **50**, 124045 (2008).
27. N. Blanchot, G. Marre, J. Néauport, E. Sibé, C. Rouyer, S. Montant, A. Cotel, C. Le Blanc, and C. Sauteret, "Synthetic aperture compression scheme for a multipetawatt high-energy laser," Appl. Opt. **45**, 6013–6021 (2006).
28. N. Blanchot, E. Bar, G. Behar, C. Bellet, D. Bigourd, F. Boubault, C. Chappuis, H. Coïc, C. Damiens-Dupont, O. Flour, O. Hartmann, L. Hilsz, E. Hugonnot, E. Lavastre, J. Luce, E. Mazataud, J. Neauport, S. Noailles, B. Remy, F. Sautarel, M. Sautet, and C. Rouyer, "Experimental demonstration of a synthetic aperture compression scheme for multi-Petawatt high-energy lasers," Opt. Express **18**, 10088–10097 (2010).
29. S. Mousset, C. Rouyer, G. Marre, N. Blanchot, S. Montant, and B. Wattellier, "Piston measurement by quadriwave lateral shearing interferometry," Opt. Lett. **31**, 2634–2636 (2006).
30. C. Rouyer, N. Blanchot, J. Neauport, and C. Sauteret, "Delay interferometric single shot measurement of a petawatt-class laser longitudinal chromatism corrector," Opt. Express **15**, 2019–2032 (2007).
31. J. Néauport, N. Blanchot, C. Rouyer, and C. Sauteret, "Chromatism compensation of the PETAL multipetawatt high-energy laser," Appl. Opt. **46**, 1568–1574 (2007).
32. Y. Izawa, "Overview of FIREX Program," in *Proceedings of 5th US-Japan Workshop on Laser IFE* (2005).
33. M. Dunne, N. Alexander, and F. Amiranoff, et al., "Technical Background and Conceptual Design Report 2007," http://www.hiper-laser.org/overview/tdr/tdr.asp.
34. The ELI-Nuclear Physics working groups, "The White Book of ELI Nuclear Physics," http://www.eli-np.ro/documents/ELI-NP-WhiteBook.pdf.
35. J. W. Goodman, *Introduction to Fourier Optics*, 3rd Ed. (Roberts, 2005).
36. C. D. Nabors, "Effects of phase errors on coherent emitter arrays," Appl. Opt. **33**, 2284–2289 (1994).
37. G. Chanan, C. Ohara, and M. Troy, "Phasing the mirror segments of the Keck Telescopes II: The narrow-band phasing algorithm," Appl. Opt. **39**, 4706–4714 (2000).
38. N. Yaitskova, K. Dohlen, and P. Dierickx, "Analytical study of diffraction effects in extremely large segmented telescopes," J. Opt. Soc. Am. A **20**, 1563–1575 (2003).
39. G. Chanan and M. Troy, "Strehl ratio and modulation transfer function for segmented mirror telescopes as functions of segment phase error," Appl. Opt. **38**, 6642–6647 (1999).
40. C. A. Haynam, P. J. Wegner, J. M. Auerbach, M. W. Bowers, S. N. Dixit, G. V. Erbert, G. M. Heestand, M. A. Henesian, M. R. Hermann, K. S. Jancaitis, K. R. Manes, C. D. Marshall, N. C. Mehta, J. Menapace, E. Moses, J. R. Murray, M. C. Nostrand, C. D. Orth, R. Patterson, R. A. Sacks, M. J. Shaw, M. Spaeth, S. B. Sutton, W. H. Williams, C. C. Widmayer, R. K. White, S. T. Yang, and B. M. Van Wonterghem, "National Ignition Facility laser performance status," Appl. Opt. **46**, 3276–3303 (2007).
41. S. C. Burkhart, E. Bliss, P. Di Nicola, D. Kalantar, R. Lowe-Webb, T. McCarville, D. Nelson, T. Salmon, T. Schindler, J. Villanueva, and K. Wilhelmsen, "National Ignition Facility system alignment," Appl. Opt. **50**, 1136–1157 (2011).
42. Y.-Q. Gao, B.-Q. Zhu, D.-Z. Liu, X.-F. Liu, and Z.-Q. Lin, "Characteristics of beam alignment in a high power four-pass laser amplifier," Appl. Opt. **48**, 1591–1597 (2009).